Tellus (2000), 52B, 484–497
Printed in UK. All rights reserved

TELLUS
ISSN 0280–6509

Regional aerosol optical depth characteristics from satellite observations: ACE-1, TARFOX and ACE-2 results

By P. A. DURKEE[1]*, K. E. NIELSEN[1], P. J. SMITH[1], P. B. RUSSELL[2], B. SCHMID[3], J. M. LIVINGSTON[4], B. N. HOLBEN[9], C. TOMASI[11], V. VITALE[11], D. COLLINS[5], R. C. FLAGAN[5], J. H. SEINFELD[5], K. J. NOONE[6], E. ÖSTRÖM[9], S. GASSÓ[7], D. HEGG[7], L. M. RUSSELL[10], T. S. BATES[8] and P. K. QUINN[8], [1]*Naval Postgraduate School, Monterey, CA USA;* [2]*NASA Ames Research Center, Moffett Field, CA USA;* [3]*Bay Area Environmental Research Institute, San Francisco, CA 94122, USA;* [4]*SRI International, Menlo Park, CA 94025, USA;* [5]*California Institute of Technology, Pasadena, CA, USA;* [6]*Stockholm University, Stockholm, Sweden;* [7]*University of Washington, Seattle, WA, USA;* [8]*NOAA PMEL, Seattle, WA, USA;* [9]*NASA Goddard Space Flight Center, Greenbelt, MD, USA;* [10]*Princeton University, Princeton, NJ, USA;* [11]*FISBAT, Bologna, Italy*

(Manuscript received 9 February 1999; in final form 6 September 1999)

ABSTRACT

Analysis of the aerosol properties during 3 recent international field campaigns (ACE-1, TARFOX and ACE-2) are described using satellite retrievals from NOAA AVHRR data. Validation of the satellite retrieval procedure is performed with airborne, shipboard, and land-based sunphotometry during ACE-2. The intercomparison between satellite and surface optical depths has a correlation coefficient of 0.93 for 630 nm wavelength and 0.92 for 860 nm wavelength. The standard error of estimate is 0.025 for 630 nm wavelength and 0.023 for 860 nm wavelength. Regional aerosol properties are examined in composite analysis of aerosol optical properties from the ACE-1, TARFOX and ACE-2 regions. ACE-1 and ACE-2 regions have strong modes in the distribution of optical depth around 0.1, but the ACE-2 tails toward higher values yielding an average of 0.16 consistent with pollution and dust aerosol intrusions. The TARFOX region has a noticeable mode of 0.2, but has significant spread of aerosol optical depth values consistent with the varied continental aerosol constituents off the eastern North American Coast.

1. Introduction

Atmospheric aerosols, whether anthropogenic or naturally occurring, impact the Earth's energy budget. Incoming solar radiation is scattered by these aerosols resulting in a net decrease in heating of the Earth's surface. Aerosols provide smaller condensation nuclei that increase cloud albedo at solar wavelengths, which again reduces heating at the Earth's surface. This is important because the effect is exactly the opposite of the global warming effect attributed due to greenhouse gases. According to Charlson et al. (1992) and the Intergovernmental Panel on Climate Change (IPCC) (1996), the cooling influence caused by aerosols maybe offsetting the greenhouse warming to a substantial degree. Schwartz and Andreae (1996) point out that if the aerosol forcing is significant and has negated much of the greenhouse forcing, then the resultant increase in global temperatures has come from a small residual forcing indicating a greater planetary temperature sensitivity. A greater sensitivity may result in accelerated global warming in the future. The

* Corresponding author: 589 Dyer Road, Room 254, Monterey, CA, 93943–5113, USA.
e-mail: Durkee@nps.navy.mil.

uncertainty of aerosol forcing on the climate needs to be reduced to near the levels of uncertainty in greenhouse forcing in order to determine their relative importance. One avenue towards reducing this uncertainty is through satellite-based measurements of aerosol properties both globally and regionally.

Kiehl and Briegleb (1993) illustrated the importance of regional variability to the problem of aerosol radiative forcing. Detail characterization of aerosol optical properties can be accomplished through in situ measurements of the physical and chemical properties of aerosol distributions. Sunphotometers, spectrometers, and radiometers provide very accurate pictures of these parameters, but they are limited spatially and temporally. Satellite-based radiometers provide coverage at regional to global scales. As described here the National Oceanic and Atmospheric Administration (NOAA) Polar Orbiting Environmental Satellite (POES) with its Advanced Very High Resolution Radiometer (AVHRR) can provide up to two passes per day for local analysis and a global picture once per day. Use of AVHRR data on a global scale has been demonstrated by Husar et al. (1997) and Nakajima and Higurashi (1998). The AVHRR channel 1 (visible) and channel 2 (near infrared) possess the appropriate spatial and spectral resolution to measure optical radiative properties. This two solar channel capability is unique to the AVHRR instrument. Work done by Durkee et al (1991), Rouault and Durkee (1992) and Brown (1997) explore the use of the AVHRR two solar channel capability as a way to characterize phase scattering effects of aerosols. Aerosol retrieval techniques based on their work are used in this study.

Several experiments over the late 1990′s have focused on aerosol properties and have provided ample field data for use in studies of aerosol optical properties. These experiments include the International Global Atmospheric Chemistry (IGAC) Project's First Aerosol Characterization Experiment (ACE-1) in November 1995, Second Aerosol Characterization Experiment (ACE-2) in June 1997, and Tropospheric Aerosol Radiative Forcing Observational Experiment (TARFOX) in July 1996. These experiments are important because they provide information on several different aerosol distributions that broadly represent many of the aerosol distributions found globally. ACE-1 focused on aerosols in the remote marine atmosphere of the Southern Hemisphere; TARFOX focused on aerosols carried over the western North Atlantic Ocean from the United States; and ACE-2 focused on anthropogenically-modified aerosols and dust aerosols carried over the eastern North Atlantic Ocean from Europe and Africa.

2. Experimental measurements and procedure

In order to validate the optical depth retrieval method described in this study, reference data from ACE-2 were chosen based on the availability of surface and airborne sunphotometer measurements of optical depth. To the greatest extent possible, sunphotometer measurements are matched to satellite observations both spatially and temporally. The composite aerosol optical properties were produced using the validated AVHRR retrieval method on data collected during each of the three experiments.

2.1. Overview of experiments

The main goal of ACE-1 was to determine and understand the properties and controlling factors of aerosols in the remote marine atmosphere that are relevant to radiative forcing and climate. This experiment took place in the minimally polluted marine atmosphere of the southern ocean south of Australia from 15 November to 15 December 1995. This area was selected due to the relatively simple marine aerosol background and its distance from the Northern Hemisphere sulfate aerosols. This aerosol background can provide a baseline to compare with anthropogenically perturbed aerosols transported from the continents. Bates et al. (1998) provides an overview of ACE-1.

TARFOX was designed as a closure study to better understand the radiative forcing effects of aerosols. TARFOX was conducted in the continentally influenced environment off the eastern coast of the United States near Wallops Island, Virginia from 10–31 July 1996. During TARFOX, a variety of aerosol conditions ranging from relatively clean to moderately polluted were observed and measured (Russell et al., 1996). The TARFOX Operations Summary (Whiting et al., 1996) contains details of the field collection effort.

ACE-2 carried on the goals of ACE-1, but focused on anthropogenic aerosols from the European continent and desert dust from the African continent as they move over the North Atlantic Ocean. This experiment was carried out between 16 June and 25 July, 1997 and involved coordinated data collection by 6 aircraft, one ship, and ground stations on Tenerife, Portugal and Madeira. An overview on the ACE-2 objectives can be found in the experiment's Science and Implementation Plan (IGAC, 1995). NOAA-14 AVHRR data were collected in real-time during the exercise. Aerosol optical depth measurements from four different sunphotometers were used to validate aerosol optical depth values from the satellite retrieval. The NASA Ames Airborne Tracking Sunphotometer (AATS-14) was flown aboard the Center for Interdisciplinary Remotely Piloted Aircraft Studies (CIRPAS) Pelican aircraft. The NASA Ames Airborne Tracking Sunphotometer (AATS-6) was operated aboard the R/V Vodyanitskiy. The ground station at Tenerife used a CIMEL Electronique 318A sun/sky scanning spectral radiometer and the ground station at Sagres, Portugal used both the UVISIR-1 and IR-RAD sunphotometers.

2.2. Optical depth measurements

2.2.1. Satellite retrieval. The NOAA Advanced Very High Resolution Radiometer (AVHRR) instrument is a component of the NOAA Polar Orbiting Operational Environmental Satellite (POES) series satellites. These satellites are in Sun synchronous orbit (883 km) and provide two passes per day in the morning and evening, respectively. The NOAA-14 data were used exclusively for the composite analysis used in this study to reduce the complications from diurnal variations in the aerosol optical depth retrieval that would result from combining observations from multiple overpass times. The AVHRR instrument measures radiant and solar-reflected energy from sampled areas of the Earth in 5 spectral bands with a sub-satellite resolution of 1.1 km. Channels 1 and 2 are used in the optical depth retrieval presented here. Radiance values are derived according to the most recent updates to the pre-launch calibrations (Rao and Chen, 1995) of AVHRR Channels 1 and 2. Channels 1 through 5 are used in the cloud screening analysis.

The optical depth retrieval technique used in this study is an automated process based on work developed by Brown (1997). The procedure includes a check for sun glint, a cloud screening algorithm, and a linearized single-scatter radiative transfer estimate of optical depth. Rayleigh scattering is removed by calculating the radiance according to Turner (1973) assuming an optical depth of 0.057 for channel 1 and 0.019 for channel two. Ozone absorbtance is calculated using an optical depth of 0.027 for channel 1 and 0.0021 for channel 2. Surface reflectance is assumed to be 0.005 for channel 1 and zero for channel 2.

The sun glint check calculates the probability of sun glint in a given pixel based on the Cox and Munk (1954) model. This process takes into account sun-satellite geometry and wind speed. A conservative 14 m/s (lower values decrease the area of sunglint) was used for the wind speed over the entire image and the pixel was removed if the probability of sun glint was greater than 35% (corresponds to all scattering angles with in 15° of specular reflection). The cloud screening algorithm, based on Saunders and Kriebel (1988), applies the following tests to determine cloud contamination in a given pixel.

- Gross cloud check: The pixel was removed if the Channel 4 temperature was less than the sea surface temperature (additionally, if the channel 4 temperature was greater than 303 K the pixel was considered to be land).
- Spatial coherence: The pixel was removed if the standard deviation of the channel 4 temperature was greater than 0.1 K or the standard deviation of the channel 3 temperature was greater than 0.45 (within a 3×3 pixel box).
- Dynamic reflectance threshold test: The pixel was removed if the channel 2 reflectance was greater than 15% and if the channel 4 minus channel 5 temperature difference is greater than zero. The temperature difference test allows for a high reflectance due to dust aerosols (used only for ACE-2).
- VIS/NIR ratio test: The pixel was removed if the ratio of channel 1 to channel 2 bi-directional reflectance was less than 1.33.
- Thin cirrus test: The pixel was removed if the difference between the channel 4 and channel 5 temperatures was greater than pre-computed clear sky values.

2.2.2. Radiative transfer solution. Accurate estimates of optical depth from measurements of backscattered solar radiance require assumptions about the scattering phase function and single scatter albedo. In addition, estimates of the surface reflectance, ozone absorption and molecular scattering are required. The aerosol properties are not generally known unless in situ aerosol measurements are taken. Parameterization of the scattering phase function is necessary to solve the radiative transfer problem. The method used in this study takes advantage of the differences in the measured radiance at different wavelengths to parameterize the scattering phase function.

Durkee et al. (1991) proposed using the measured aerosol radiance differences in the AVHRR channel 1 (visible) and 2 (NIR) to parameterize the phase function. The scattering efficiency (Q_{scat}) of an aerosol distribution is wavelength-dependent; therefore, when the radius of the aerosol is nearly equal to the radiation wavelength, Q_{scat} is a maximum. The ratio of the channel 1 and 2 radiances will be larger for smaller size particle distributions and smaller for larger size particle distributions. Durkee et al. (1991) called this ratio the particle size parameter, S_{12}. Since S_{12} varies in each pixel of the satellite image, the scattering phase functions can be parameterized for each pixel, allowing variations in aerosol distributions in the optical depth retrieval.

7 model aerosol size distributions (based on Brown, 1997) were created to represent a range of variations of aerosol in the marine environment. Model M0 is a single mode distribution with mode radius 0.1 μm and standard deviation of 0.7. Models M1–M6 are combinations of M0 with varying second modes with mode radius 0.3 μm and standard deviations: $M1 = 2.1$, $M2 = 2.2$, $M3 = 2.35$, $M4 = 2.51$, $M5 = 2.6$, and $M7 = 2.7$. The real index of refraction for the models is 1.4 (same as Ignatov, 1995).

Fig. 1 illustrates the links between the aerosol model distributions and the resulting phase functions. The scattering phase functions and radiance ratios (S_{12}) for these models were calculated using Mie theory. S_{12} is corrected for water vapor absorption in AVHRR channel 2 after Mahony (1991) using the split-channel (channels 4 and 5)

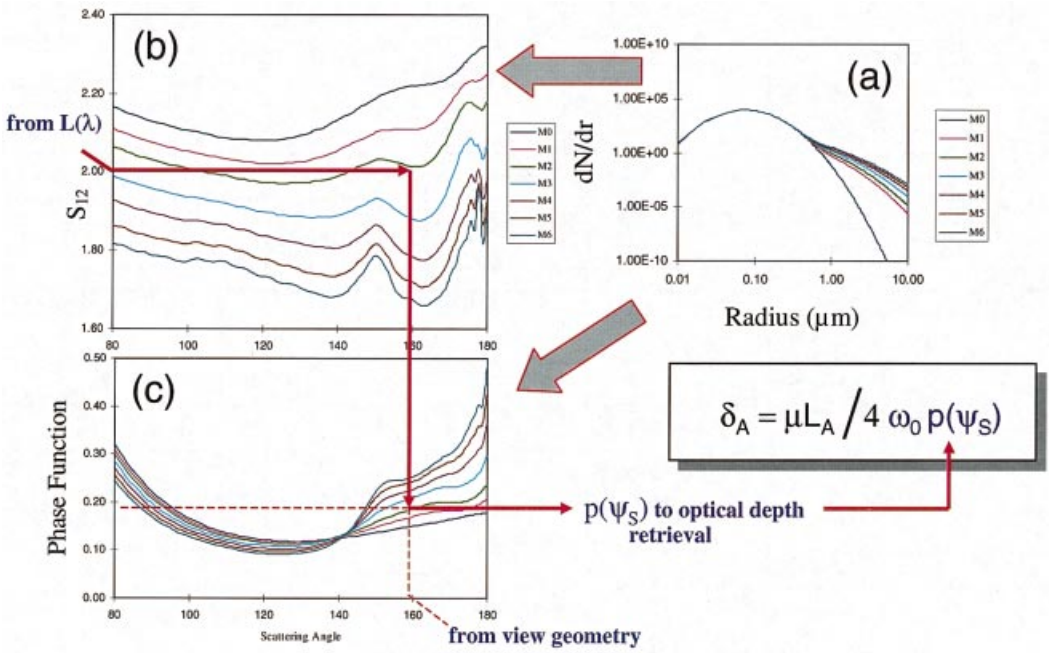

Fig. 1. Parameterization of the scattering phase function, $p(\psi_S)$, is described. (a) Aerosol model size distributions. (b) Size index, S_{12}, calculated from the extinction produced by the model size distributions as a function of scattering angle. (c) Scattering phase function calculated from the model size distributions as a function of scattering angle.

water vapor retrieval proposed by Dalu (1986). S_{12} values are calculated for each pixel from AVHRR channel 1 and channel 2 radiances. The difference between the observed and the nearest model S_{12} value is determined for the given scattering angle. Phase function values are then selected by interpolation between the model phase function values.

An additional check was added for extremely low optical-depth environments. In these cases (only observed during ACE-1 and ACE-2), the measured aerosol radiance was close to the minimum detectable radiance level. Therefore, inaccuracy in the digital brightness count of channel 2 (lower value than channel 1) could produce unrealistically high ratio values and an incorrect aerosol model assumption. In these cases, defined by channel 1 brightness counts less than 2.5 above the minimum count (equivalent to zero radiance), the aerosol model was set to M6.

Given a value for scattering phase function the optical depth is a linear function of the radiance due to aerosol scattering (L_A) according to the Linearized Single Scattering approximation (Durkee, 1991) as shown in Fig. 1. The same procedure is followed to produce an optical depth estimate for both channel 1 and channel 2 (separate phase functions are calculated according to each channel wavelength). The linearized single scattering approximation has the advantage of being an analytical solution but does not fully account for the effects of multiple scattering (within the uncertainty of AVHRR radiance measurements) above optical depths of about 0.4. Since absorption properties are unknown for individual pixels, single scattering albedo (ω_0) is assumed to be 1 for all cases presented here. The effects of this assumption are easily derived since optical depth is linearly related to ω_0.

2.2.3. Composite process. The composite process consisted of grouping pixel values into 10 by 10 km bins and performing statistical calculations. The values calculated by the radiative transfer code for each NOAA 14 pass during the exercise were summed and averaged over a bin. Since the AVHRR resolution is approximately 1 km, there could be as many as 100 pixels per bin. Some manual and automated quality control was used. Each pass was manually screened for obvious errors such as optical depth values within the boundaries of a cloud field. One hundred pixels from each side of the image (2048 pixels total) are removed to avoid sampling data from the edges of the pass where distortion exists. Summing all of the passes then created the area composite.

3. Results

3.1. Validation

The satellite retrieval was validated by comparing with sunphotometer aerosol optical depth data collected during ACE-2. 5 different instruments collected sunphotometer data at various times and places throughout the exercise period as part of the CLEARCOLUMN focus of ACE-2 described by Russell and Heintzenberg (2000). The sunphotometer data used were correlated both spatially and temporally with the retrieved data to the greatest extent possible. Comparisons were made at 630 nm and 860 nm. In all cases the sunphotometer data were linearly interpolated to these wavelengths. The uncertainty associated with the resolution of the satellite radiance measurements results in an average aerosol optical depth uncertainty of ± 0.02 based on Brown (1997).

A CMEL Electronique 318A sunphotometer, operated by AERONET, was located at the Tenerife ground station. This station was located near Punta del Hidalgo at 28°N 16.6°W and an elevation of 10 m. Retrieved aerosol optical depth data from the nearest pixel just off the coast from this ground station were used in the comparison. The sunphotometer data set was prescreened for clouds by AERONET. 8 matches to retrieved aerosol optical depth data were found between 30 June and 18 July. The time difference between retrieved values and sunphotometer values ranged between zero and 39 min. An error of ± 0.01 is associated with the aerosol optical depth measured by this instrument (Holben 1998).

The ground station at Sagres, Portugal was located at the coastal military base Radio Naval de Sagres, 37°N 8.9°W and elevation 50 m. 2 sunphotometers, UVISIR-1 and IR-RAD, were operated at this station by FISBAT (Vitale et al., this issue). Retrieved aerosol optical depth data from the nearest pixel just off the coast from this ground station were used in the comparison. Two matches to retrieved aerosol optical depth were found for the 11 and 12 July data from the

UVISIR-1 instrument. Seven matches to the retrieved aerosol optical depth data were found between 22 June and 12 July from the IR-RAD instrument. The differences in numbers of matches resulted from variable operations of the two instruments. Errors were assigned a value of ± 0.01.

NASA Ames operated the AATS-6 aboard the R/V Vodyanitsky (Livingston, 2000). The ship spent most of its underway time south of Sagres outside the Strait of Gibraltar, but in one coordinated experiment the ship traveled farther south off the coast of Morocco. Aerosol optical depth values from this sunphotometer were screened for clouds and ship mast interference. Two matches were found, one on 24 June and one on 25 June, during the time when the ship was outside the Strait of Gibraltar (35.6°N 9.2°W and 36.1°N 9.0°W respectively). The temporal agreement in these cases is good. One match was found for 10 July when the ship was off the coast of Morocco (29.3°N 11.9°W). There is a 21-min difference in the data times for this match, but this is considered acceptable since the ship moves a very short distance and the aerosol loading can be assumed to be consistent over this time. The error associated with the AATS-6 aerosol optical depth values are between ± 0.006 and ± 0.008.

The AATS-14 was flown aboard the CIRPAS Pelican aircraft (Schmid et al., 2000). The majority of flights were in clear air masses nearby the Island of Tenerife, but one flight was near the coast of Morocco in order to coordinate with ship measurements. The aircraft flew at many altitudes due to the requirement of other instrumentation onboard. The aerosol optical depth values used for comparison were only those calculated when the plane was at an altitude of 100 m or less and near the time of the satellite retrieval. For this short period of time (6 min or less) the aerosol optical depth values were averaged and the average was used as a single value for comparison. Three matches were found for this data set: 21 June near 28.9°N 17.2°W had a temporal difference of less than 11 min, 10 July near 29°N 11.13°W had a temporal difference of less than 13 min, and 17 July near 27.8°N 16.6°W had a temporal difference of less than 34 min. The error associated with the AATS-6 aerosol optical depth values are between ± 0.004 and ± 0.008.

Some retrieved aerosol optical depth data were not used even though there were matches to sunphotometer data. In areas contaminated by sun glint or clouds, the retrieval process automatically threw retrieved aerosol optical depth values away. Aerosol optical depth values that were near the edge of the satellite pass (defined by 100 pixels in the composite process) were not considered valid. Finally, retrieved values that had valid sunphotometer matches but were in a strong gradient of aerosol optical depth were not used. Strong gradients of retrieved aerosol optical depth, doubling or tripling of the aerosol optical depth value over a few pixels, are suspect for matches because they may be inconsistent both spatially and temporally with the sunphotometer aerosol optical depth or may be susceptible to cloud contamination.

The resultant data set is shown in a scatter plot in Fig. 2. There is very good agreement in the lower optical depth range for all sources and both wavelengths. In the optical depth range greater than 0.3 the satellite values are about 10% below the sunphotometer values. Since these high aerosol optical depth values are primarily due to desert dust aerosol, the bias may be due to the non-absorbing aerosol assumption made in the satellite retrieval method. If aerosol absorption were included the retrieved aerosol optical depth values would be higher and correlate more closely with the sunphotometer aerosol optical depth. Dust aerosols

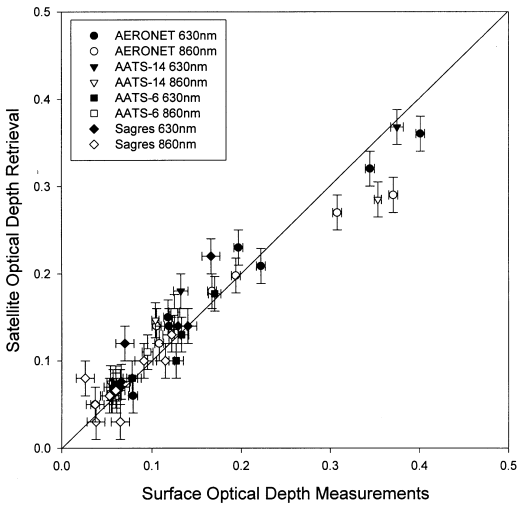

Fig. 2. Scatter diagram of surface measured aerosol optical depth versus aerosol optical depths retrieved from satellite. The correlation is 0.88 and the standard 0.02 for both wavelengths.

typically have single scatter albedo values of 0.9 or less (Ignatov et al., 1995) — consistent with the observed difference since the satellite-retrieved aerosol optical depth varies linearly with single scatter albedo. Even with this problem the correlation coefficient has a value of 0.93 for 630 nm wavelength and 0.92 for 860 nm wavelength. The standard error of estimate is 0.025 for 630 nm wavelength and 0.023 for 860 nm wavelength — only slightly greater than the uncertainty in satellite-retrieved optical depth of 0.02. Brown (1997) using data from TARFOX, also achieved a positive validation of this aerosol optical depth retrieval method.

3.2. *Regional analysis*

The regional composite images can be seen in Figs. 3–6. The composites cover larger areas than the actual exercise areas in order to identify possible sources and transport of aerosols. Figs. 3 and 4a–c are images of aerosol optical depth, at 630 nm and 860 nm respectively, for the three exercise areas. The patterns of optical depth are generally consistent with the global analysis of Husar et al. (1997) showing the desert dust plume extending westward from Africa, the continental plume extending northeastward from North America, and the relatively low optical depth values south of Australia. Fig. 5a–c are composite images of aerosol optical depth ratio. The ratio of aerosol optical depth at two different wavelengths is related to slope of the aerosol size distribution. Higher ratio values indicate areas of steeper size distribution, usually due to pollution or biomass burning, and lower values indicate marine and dust aerosols (Nakajima and Higurashi, 1998).

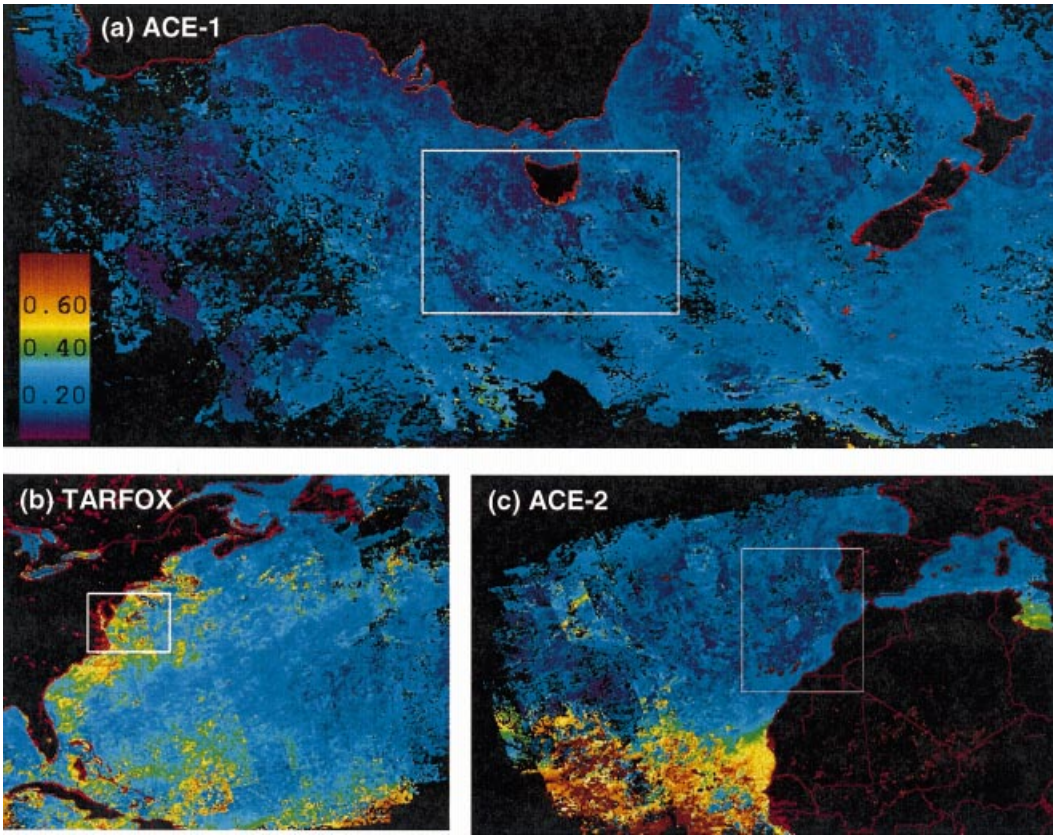

Fig. 3. Composite of aerosol optical depth at 630 nm wavelength retrieved from NOAA-14 AVHRR on 10 km grid for (a) ACE-1, (b) TARFOX, and (c) ACE-2. The white boxes define the area of operations and limit the region used for frequency distributions shown in Figs. 6, 7.

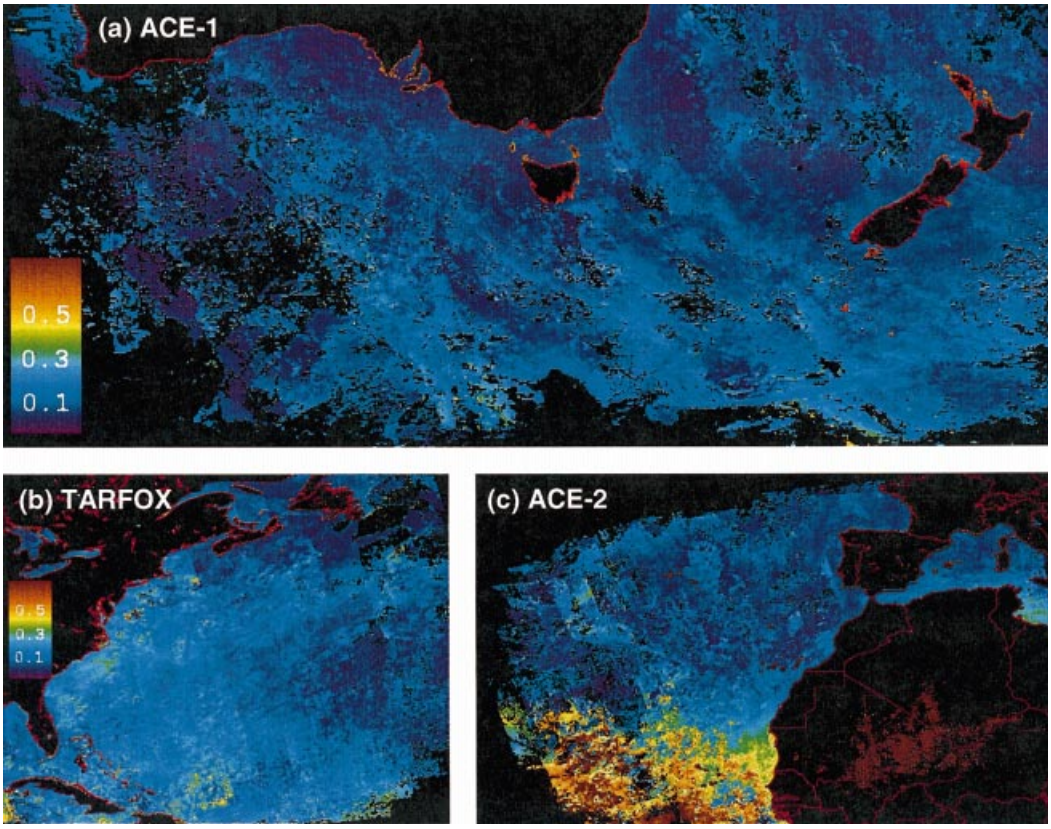

Fig. 4. Composite of aerosol optical depth at 860 nm wavelength retrieved from NOAA-14 AVHRR on 10 km grid for (a) ACE-1, (b) TARFOX, and (c) ACE-2.

Fig. 6a–c are images of the number of pixels per bin that were used in the composites. Higher numbers correlate to areas that were generally cloud free and not affected by sun glint.

The frequency distribution of optical depths and wavelength ratios for the exercise areas are shown in Figs. 7, 8. The data used in the frequency distribution are limited to only the operational areas of each exercise as described above. The mean, mode and standard deviations of the distributions are listed in Table 1.

3.2.1. ACE-1. The ACE-1 study area, defined by research aircraft and ship operations, was between 40°–55°S and 135°–160°E. During the field operations period there was an above average occurrence of cold frontal passages. A long wave trough passed over the exercise area during the course of the experiment. This led to strong west-

Table 1. *Analysis of frequency distributions of composite aerosol optical depth and wavelength ratio at 630 and 860 nm wavelength*

	Mean	Mode	SD	
aerosol optical depth at 630 nm	ACE-1	0.130	0.115	0.028
	TARFOX	0.353	0.185	0.148
	ACE-2	0.162	0.095	0.109
aerosol optical depth at 860 nm	ACE-1	0.111	0.097	0.027
	TARFOX	0.271	0.155	0.112
	ACE-2	0.140	0.075	0.096
aerosol optical depth ratio	ACE-1	1.208	1.125	0.072
	TARFOX	1.291	1.155	0.119
	ACE-2	1.150	1.025	0.119

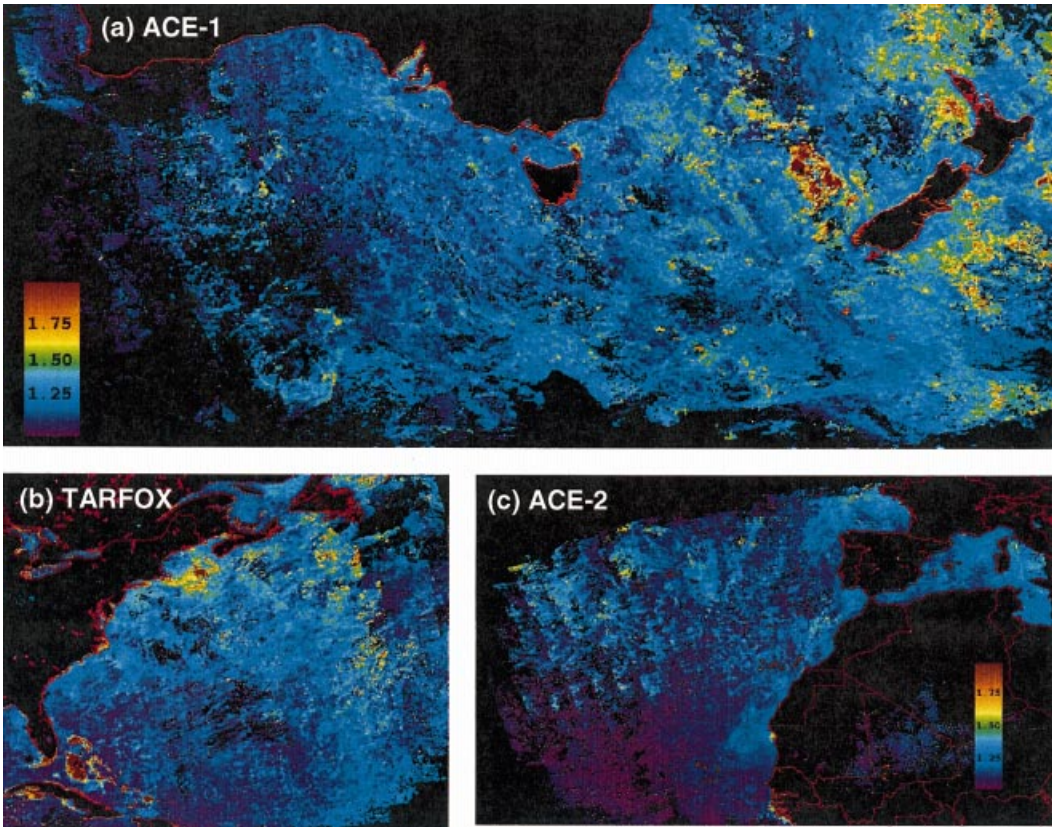

Fig. 5. Composite of aerosol optical depth wavelength ratio (630nm/860nm) retrieved from NOAA-14 AVHRR on 10 km grid for (a) ACE-1, (b) TARFOX, and (c) ACE-2.

erly to northwesterly flow in November and southerly to southwesterly flow in December. Sea salts dominate aerosol properties in this area (Hainsworth et al., 1998). As expected the aerosol optical depth (Fig. 3a and 4a) is low over most of the area with a mean of 0.13 at 630 nm and 0.11 at 860 nm. This is consistent with the assumption that continental aerosols are not the primary influence in this area. Individual images of retrieved aerosol optical depth from early in the exercise period revealed higher aerosol optical depth off the East Coast of Australia consistent with continental aerosols being advected by the observed westerly winds. Some high aerosol optical depth ratio values shown in Fig. 5a are scattered over the eastern portion of the composite. This probably indicates transport of anthropogenic aerosols into this area from the Australian continent. The standard deviation is low with a mean of 0.028 at 630 nm and 0.064 at 860 nm. This is indicative of the relatively homogenous aerosol properties in this area.

3.2.2. TARFOX. TARFOX was conducted in the continentally influenced environment off the East Coast of the United States near Wallops Island, Virginia. A variety of aerosol conditions, from relatively clean to moderately polluted, were observed. A persistent upper-level trough created extensive cloudiness on many days and highly variable haze conditions due to frequent shortwave weather systems passing over the area. Additionally, Hurricane Bertha threatened the exercise area for three days. The TARFOX composites extend south and east in order to identify aerosol sources from sub-tropical latitudes and aerosol transport across the North Atlantic Ocean. The mean values from these composites are 0.353

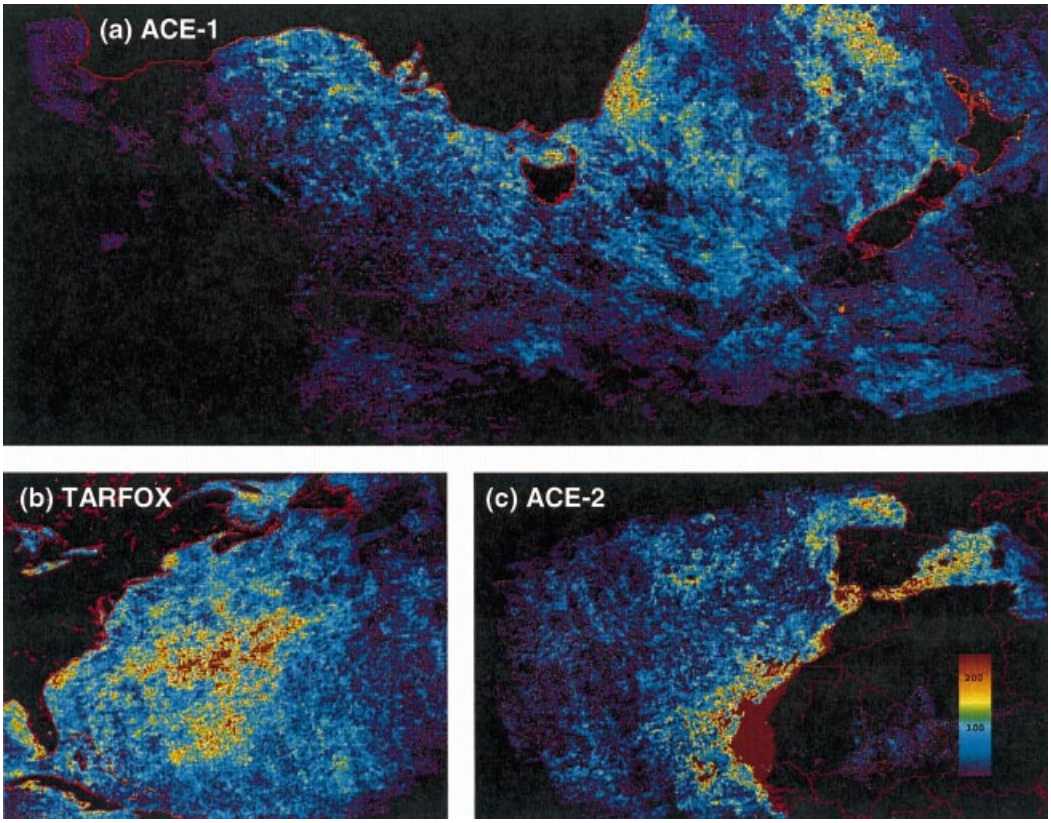

Fig. 6. Composite of number of observations per 10 km bin (a) ACE-1, (b) TARFOX, and (c) ACE-2.

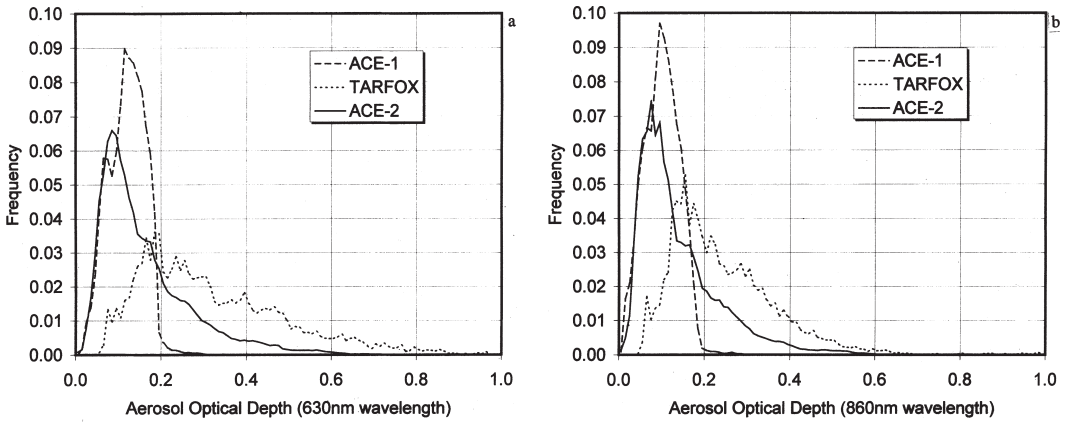

Fig. 7. Frequency distributions of aerosol optical depth within the area of operation (defined by the boxes in Fig. 2) at (a) 630 nm and (b) 860 nm wavelength for ACE-1, TARFOX and ACE-2.

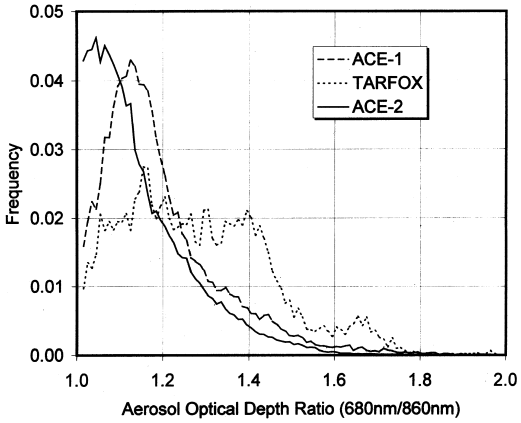

Fig. 8. Frequency distributions of aerosol optical depth wavelength ratio within the area of operation (defined by the boxes in Fig. 2) for ACE-1, TARFOX and ACE-2.

at 630 nm and 0.271 at 860 nm. These higher values are consistent with sources continental and pollution aerosols. Another source is mineral dust that originates in North Africa. The dust is transported across the sub-tropical North Atlantic Ocean by prevailing trade winds. A portion of the dust then gets entrained in the mid-latitude westerly flow. The aerosol optical depth ratio shown in Fig. 5b is high near areas where pollution aerosols are expected, specifically off the coast of major cities in the Northeastern U.S. This observed feature, due mainly to the increased amount of small aerosol particles from combustion processes, persists well into the North Atlantic Ocean. The mean values of aerosol optical depth standard deviation for this region were 0.148 at 630 nm and 0.112 at 860 nm. The relatively high standard deviation of aerosol optical depth illustrates the high variability of the aerosol conditions associated with the TARFOX region.

3.2.3. ACE-2. The ACE-2 area was selected based on its exposure to various aerosol types, including clean marine conditions, anthropogenic aerosol from Europe and desert dust. The main study area was between 23°–44°N and 8°–25°W. The composite area extends farther west into the North Atlantic Ocean and east into the Western Mediterranean Sea. The mean aerosol optical depth values are 0.142 at 630 nm and 0.126 at 860 nm. This is consistent with most of the area being dominated by clean marine aerosol. The most significant feature is the long plume of high aerosol optical depth that extends off the African continent into the North Atlantic Ocean. Aerosol optical depth values approaching 1.0 are common in this plume. An anomalous area of high aerosol optical depth is present in the northwest corner of the composite. This may be seen in time-lapse imagery as an extension of the African dust plume that has been caught in the mid-latitude westerlies or aerosols that were transported from the Western Atlantic around the sub-tropical high. Aerosol optical depth plumes extending off the coast of Algeria and Tunisia into the Mediterranean Sea are associated with dust carried by Sirocco winds. There is some evidence of pollution out breaks, based on higher aerosol optical depth, south and west of Portugal. These events are seen periodically in individual cases, but are averaged out over time in the composite. The standard deviation of aerosol optical depth was 0.064 at 630 nm and 0.061 at 860 nm. The aerosol optical depth ratio is low and fairly consistent over the entire area. North of the dust plume the ratio values increase which may be a result of pollution aerosols from the European continent. The standard deviation values are influenced by large standard deviation values in the area of the African dust plume.

The frequency distribution plots in Fig. 7 for ACE-1 and ACE-2 have a similar profile with modes of 0.115 and 0.095 (at 630 nm) respectively. It is interesting that the ACE-2 frequency plot has a lower mode than the ACE-1 plot even though the mean aerosol optical depth in the ACE-2 composite is larger. The mean value for ACE-2 is driven higher by the effect of the European pollution and the African dust plume in ACE-2 which results in a tail in the distribution toward higher values of aerosol optical depth.

4. Conclusions

A satellite-based retrieval procedure using NOAA POES AVHRR is used to analyze the optical properties of aerosols in regions studied during recent international field measurement programs. Retrieved satellite aerosol optical depth was compared to surface-measured sun-photometer aerosol optical depth collected during the International Global Atmospheric Chemistry (IGAC) Project's Second Aerosol

Characterization Experiment (ACE-2) from 16 June to 25 July 1997. Sunphotometer data from four independent sites were used in the comparison, ground stations at Tenerife Island and Sagres, Portugal, AATS-6 on board the R/V Vodyanitskiy, and AATS-14 on board the CIRPAS aircraft Pelican. There was good agreement between the aerosol optical depth retrieved from satellite and those measured by sunphotometer, especially at low values of aerosol optical depth. At higher values of aerosol optical depth the retrieved values are low, but this is most probably due to the no-absorption assumption made in the retrieval. The comparison data set has a correlation coefficient of 0.93 and 0.92 with a standard error of 0.025 and 0.023 at 630 nm and 860 nm wavelengths, respectively. This indicates a positive validation of the retrieval method. The retrieval technique is assumed to validate for the ACE-1 area and is used for the regional analysis discussed below.

Regional aerosol properties are examined with an emphasis on the differences between the ACE-1, TARFOX and ACE-2 regions. Aerosol optical depths determined from satellite retrieval were averaged for the duration of the exercise periods and combined into composite images at 10×10 km resolution. Statistics were also calculated for each exercise area. The images give a good indication of aerosol loading under cloud-free conditions as well as source and transport regions in each area. The comparison of the three experiments provides important regional-scale context to investigators studying local-scale aerosol processes and provides an assessment of the aerosol differences between these experiments.

Aerosol optical depth retrievals from satellites do not tell the whole story. These observations are valid for cloud-free conditions and therefore may be biased if aerosol sources and transport processes are correlated with cloud conditions. During ACE-2 three European pollution outbreaks occurred under relatively cloudy conditions (Johnson et al., this issue). Although higher optical depths are detected within cloud gaps during these outbreaks and included in the composite analysis, the stratocumulus cloud cover reduces the areal extent of the high optical depth regions.

Aerosol optical depth frequency plots are used to identify regional differences of the three exercises. ACE-1 and ACE-2 regions have strong modes at aerosol optical depth at around 0.1, but ACE-2 tails toward higher values consistent with urban and dust aerosol intrusion. The TARFOX region has a noticeable mode at aerosol optical depth around 0.2, but has significant spread of aerosol optical depth values consistent with the varied aerosol constituents in that area.

These results are directly applicable to aerosol radiative forcing assessments. Russell (1998) describes column closure experiments carried out during ACE-2 showing the consistency between column radiative effects and aerosol physical and optical properties. The results presented here extend the optical properties of the column to the regional scale — at least to the extent of a two-wavelength average optical depth plus variability. Combining these results with in situ assessments of absorption properties of the aerosol will allow calculation of direct radiative forcing and its variability.

5. Acknowledgements

This study was funded by grants from Office of Naval Research, the National Science Foundation, and the European Commission. Francisco J. Exposito and Juan P. Diaz of Universidad de La Laguna, Tenerife, Canary Islands graciously provided additional AVHRR files from their archive to supplement the ACE-2 data set. This research is a contribution to the International Global Atmospheric Chemistry (IGAC) Core project of the International Geosphere–Biosphere Programme (IGBP) and is part of the IGAC Aerosol Characterization Experiments (ACE).

REFERENCES

Bates, T. S., Huebert, B. J., Gras, J. L., Griffiths, F. B. and Durkee, P. A. 1998. International Global Atmospheric Chemistry (IGAC) Project's First Aerosol Characterization Experiment (ACE 1): Overview. *J. Geophys. Res.* **103**, 16297–16318.

Brown, B. B. 1997. *Remote measurement of aerosol optical properties using the NOAA POES AVHRR and GOES imager during TARFOX*. MS thesis, Naval Postgraduate School, Monterey, CA, 73 pp.

Charlson, R. J., Swartz, S. E., Hales, J. M., Cess, R. D.,

Coakley, J. R. Jr., Hansen, J. E. and Hoffman, D. J. 1992. Climate forcing by anthropogenic aerosols. *Science* **255**, 423–430.

Cox, C. and Munk, W. 1954. Measurements of the roughness of the sea surface from photographs of the sun's glitter. *J. Opt. Soc. Am.* **44,** 838–850.

Dalu, G. 1986. Satellite remote sensing of atmospheric water vapor. *Int. J. Rem. Sen.* **7**, 1089–1097.

Durkee, P. A., Pfeil, F., Frost, E. and Shema, R. 1991. Global analysis of aerosol particle characteristics. *Atmos. Env.* **25A**, 2457–2471.

Elterman, L. 1970. *Vertical-attenuation model with eight surface meteorological ranges 2 to 13 km.* AFCRL-70-0200 Air Force Cambridge Research Laboratory, Cambridge, MA, 56 pp.

Gordon, H. R. and Clark, D. K. 1980. Atmospheric effects in the remote sensing of phytoplankton pigments. *Boundary Layer Met.* **18**, 299–313.

Hainsworth, A. H. W., Dick, A. L. and Gras, J. L. 1998. Climatic context of the First Aerosol Characterization Experiment ACE (1): A meteorological and chemical overview. *J. Geophys. Res.* **103**, 16319–16340.

Holben, B. N., Eck, T. F., Slutsker, I., Tanre, D., Buis, J. P., Setzer, A., Vermote, E., Reagan, J. A., Kaufman, Y. J., Nakajima, T., Lavenu, F., Jankowiak, I. and Smirnov, A. 1998. AERONET-A federated instument network and data archive for aerosol characterization. *Rem. Sen. Env.* **66**, 1–16.

Husar, R., Prospero, J. and Stowe, L. L. 1997. Characterization of tropospheric aerosols over the oceans with the NOAA/AVHRR optical thickness operational product. *J. Geophys. Res.* **102**, 16,889–16,910.

Intergovernmental Panel on Climate Change (IPCC) 1996. *Climate Change 1995*, J. T. Houghton et al. (eds.). Cambridge University Press, New York.

IGAC 1995. *International global atmospheric chemistry project, north Atlantic Aerosol Characterization Experiment (ACE-2). Radiative forcing due to anthropogenic aerosols over the north Atlantic region. Science and implementation plan.* European Commission DG XIII, Report No. CL-NA-16229-EN-C. 112 pp.

Ignatov, A. M., Stowe, L. L., Sakerin, S. M. and Korataev, G. K. 1995. Validation of the NOAA/NESDIS satellite aerosol product over the North Atlantic in 1989. *J. Geophys. Res.* **100**, 5123–5132.

Kidwell, K. B. 1995. *NOAA Polar orbiter data users guide.* National Environmental Satellite, Data, and Information Service (NESDIS), National Oceanic and Atmospheric Administration, 394 pp.

Kiehl, J. T. and Briegleb, B. P. 1993. The relative roles of sulfate aerosols and greenhouse gases in climate forcing. *Science* **260**, 311–314.

Koepke, P. 1984. Effective reflectance of ocean whitecaps. *Appl. Opt.* **23**, 1816–1824.

Livingston, J. M. and Russell, P. B. 1997. Aerosol optical depth spectra, vertical profiles, and horizontal transects derived from TARFOX airborne sunphotometer measurements, EOS. *Trans. Amer. Geophys. Union* **78**, S92.

Livingston, J. M., Kapustin, V., Schmid, B. Russell, P. B., Durkee, P. A., Bates, T. S., Quinn, P. K., Smith, P. J., Freudenthaler, V., Covert, D. S., Gassó, S., Hegg, D., Collins, D. R., Flagan, R. C., Seinfeld, J. H., Vitale, V. and Tomasi, C. 2000. Shipboard sunphotometer measurements of aerosol optical depth spectra and water vapor during ACE-2 and comparison with selected land, ship, aircraft, and satellite measurements. *Tellus* **52B**, 494–619.

Mahony, T. P. 1991. *Water vapor influence on satellite-measured aerosol characteristics.* MS thesis. Naval Postgraduate School, Monterey, CA, 43 pp.

Matsumoto, Y., Mina, C., Russell, P. B. and Vanark, W. B. 1987. *Airborne tracking sunphotometer apparatus and system.* NASA Technical Report 1988005110 N (88N14492). NASA Ames Research Center, Moffett Field, CA, 10 pp.

Nakajima, T. and Higurashi, A. 1998. A use of two-channel radiances for aerosol characterization from space. *Geophys. Res. Let.* **25**, 3815–3818.

Ramsey, R. C. 1968. *Study of the remote measurement of ocean color.* Final Report, TRW, NASW-1658, 94 pp.

Rao, C. R. N. and Chen, J. 1995. Inter-satellite calibration linkages for the visible channels of the Advanced Very High Resolution Radiometer on the NOAA-7, -9, and -11. *Int. J. Rem. Sen.* **16**, 1931–1942.

Rouault, M. and Durkee, P. A. 1992. Characterization of aerosols from satellite remote sensing. In: *Nucleation and atmospheric aerosols*, pp. 357–360, N. Fukuta and P. E. Wagoner (eds.). A. Deepak Publishing.

Russell, P. B., Whiting, W., Hobbs, P. V. and Stowe, L. L. 1996. *Tropopsheric aerosol radiative forcing observational experiment (TARFOX) science and implementation plan.* NASA Ames Research Center, Moffett Field, CA, 50 pp.

Russell, P. B., Livingston, J. M., Schmid, B., Chien, A., Gasso, S., Hegg, D. A., Noone, K. J., Collins, D., Jonsson, H., Nielsen, K. E., Durkee, P. A., Flagan, R. C., Seinfeld, J. H., Bates, T. S. and Quinn, P. K. 1998. Clear column closure studies of urban-marine and mineral-dust aerosols using aircraft, ship, and satellite measurements in ACE 2. *J. Aerosol Sci.* **29**, S1143–S1144.

Russell, P. B. and Heintzenberg, J. 2000. An overview of the ACE 2 clear sky column closure experiment (CLEARCOLUMN). *Tellus* **52B**, 463–483.

Saunders, R. W. and Kriebel, K. T. 1988. An improved method for detecting clear sky and cloudy radiances from AVHRR data. *Int. J. Rem. Sen.* **9**, 123–150.

Schmid, B., Livingston, J. M., Russell, P. B., Durkee, P. A., Collins, D. R., Flagan, R . C., Seinfeld, J. H., Gasso, S., Hegg, D. A., Ostrom, E., Noone, K. J., Welton, E. J., Voss, K., Gordon, H. R., Formenti, P. and Andreae, M., O. 2000. Clear sky closure studies of lower tropospheric aerosol and water vapor during ACE-2 using airborne sunphotometer, airborne in-situ, space-borne, and ground based measurements. *Tellus* **52B**, 568–593.

Swartz, S. E. and Andeae, M. O. 1996. Uncertainty in climate change by aerosols. *Science* **272**, 1121–1122.

Turner, R. 1973. Atmospheric effects in remote sensing. In: *Remote sensing of the earth's resources* (II), pp. 549–583, F. Shahrocki (ed.). University of Tennessee.

Vitale, V., Tomasi, C., Bonafé, U., Marani, S., Lupi, A., Cacciari, A. and Ruggeri, P. 2000. Spectral measurements of aerosol particle extinction in the 0.4–3.7 micrometer wavelength range, performed at Sagres with the IR-RAD sunradiometer. *Tellus* **52B**, 716–733.

Whiting, W., Russell, P. B., Hobbs, P. V. and Stowe, L. L. 1996. *Tropospheric aerosol radiative forcing observational experiment (TARFOX) operations summary*. International Global Atmospheric Chemistry Project (IGAC), 127 pp.